NRL Report 7292

VHF Antennas for Low-Altitude Satellites

STEPHEN NICHOLS

Space Systems Division

July 12, 1971

NAVAL RESEARCH LABORATORY
Washington, D.C.

Approved for public release; distribution unlimited.

CONTENTS

Abstract	ii
Problem Status	ii
Authorization	ii
INTRODUCTION	1
DERIVATION OF THEORY	1
Turnstile Antenna Theory	1
Calculated and Measured Patterns	3
APPLICATION OF THE THEORY	11
Solar Explorer C	11
Turnstile on a Boom	21
ANOTHER APPROACH	40
Orbital Analysis	40
The Array Antenna	44
Array Summary	48
CONCLUSION	48
ACKNOWLEDGMENTS	49
BIBLIOGRAPHY	50
APPENDIX—Glossary of Symbols and Terms	51

ABSTRACT

Two vhf satellite antennas are discussed in depth. The first is a turnstile antenna, which is presented with theory, computer calculations, experimental results, and two novel applications. The first application solves the problem of interfering solar cell panels by combining them with the antenna. The second application puts the turnstile antenna on a boom away from the satellite to minimize interference.

The second vhf satellite antenna presented has multiple elements and is designed to optimize the pattern with respect to the distance and angle from a stabilized satellite to a ground station as it passes overhead. This antenna was found to have a 3-dB improvement over the best turnstile designs.

PROBLEM STATUS

This is an interim report on one phase of a continuing problem.

AUTHORIZATION

NRL Problems A01-17 and A01-20
Project A37-538-002/652-1/F019-01-01

Manuscript submitted April 15, 1971.

VHF ANTENNAS FOR LOW-ALTITUDE SATELLITES

INTRODUCTION

This report is a sequel to NRL Report 6907.* It has a more detailed study of the theory of turnstile antennas and orbital effects, and it presents the results of tests on one recently launched satellite and two proposed satellites. There are three sections, the first of which is on turnstile antenna theory, including polarization effects, calculated and measured patterns, and comparisons between the latter. The second section presents the application of the turnstile antenna on two satellites, one launched in 1969 and one launched in 1971. Both of these satellites have unique and new applications of the turnstile antenna. The third section presents an orbital analysis with respect to rf communications and a new approach to the problem of a vhf antenna for a low-altitude satellite.

DERIVATION OF THEORY

Turnstile Antenna Theory

The turnstile antenna has been used for more spacecraft than any other. Its omnidirectional coverage enables the designer to separate the problems of stabilization from the problems of data and command transmission. To better understand the application of the turnstile antenna, a theory has been developed, which, with the use of a digital computer, allows the comparison of observed and calculated results, and aids in the prediction of design goals to be used in planning future satellite designs.

The turnstile antenna comes closest to having omnidirectional coverage. However, while the power varies but little, the polarization changes considerably over the sphere. It is therefore necessary to describe the power pattern and polarization efficiency of the antenna to understand it fully. The received signal transmitted from a turnstile antenna can vary over a wide range depending on whether the receiving antenna is linearly or circularly polarized.

The form of the turnstile antenna is that of two crossed dipoles, fed in phase quadrature. The antenna pattern for the dipole may be expressed as

$$E = \frac{\cos\left[(\Pi/2)\cos\phi\right]}{\sin\phi},$$

where E is the relative field. For the turnstile antenna, the two dipole patterns are combined and the expression for the relative field is

$$E(\phi, t) = \frac{\cos\left[(\Pi/2)\cos\phi\right]}{\sin\phi}\cos\omega t + \frac{\cos\left[(\Pi/2)\sin\phi\right]}{\cos\phi}\sin\omega t.$$

*S. Nichols, "Satellite Turnstile Antennas," NRL Report 6907, Aug. 6, 1969.

At any instant of time the pattern is a figure eight of the same shape as that of a dipole. The rotation is at a rate of $\phi = \omega t$. The time-invariant version of this formula is

$$E(\phi) = \sqrt{\left\{\frac{\cos[(\Pi/2)\cos\phi]}{\sin\phi}\right\}^2 + \left\{\frac{\cos(\Pi/2\ \sin\phi)}{\cos\phi}\right\}^2}.$$

However, this formula describes the antenna pattern only in the plane of the turnstile. In the axial direction the power is constant and $E = \sqrt{1^2 + 1^2} = 1.41$. It is more convenient to talk in terms of relative power than relative field, where $P(\phi) = E^2(\phi)$. The complete expression for relative power over the sphere for a turnstile antenna is

$$P(\phi, \theta) = \left[E(\phi)^2\ \frac{1+\cos 2\theta}{2} + \frac{1-\cos 2\theta}{2}\right]\left(1+\left\{\frac{\cos[(\Pi/2)\cos\theta]}{\sin\theta}\right\}^2\right)$$

where ϕ is the notation in the plane of the turnstile and θ is the orthogonal notation about the plane of the turnstile.

To complete the description of the antenna, the polarization efficiency must be calculated. By using the Poincaré sphere a general formula may be developed:

$$\Gamma = \frac{1 + P_w^2 P_R^2 + 2\ P_w P_R \cos D}{(1 + P_w^2)\ (1 + P_R^2)},$$

where Γ is the polarization efficiency (a power term), P_w is the polarization of the incoming wave, P_R is the polarization of the receiving antenna, and D is the polar angle of separation of the two polarizations on the Poincaré sphere. In this case the receiving antenna will be the turnstile antenna and the incoming wave will be one of four separate polarizations normally used by ground stations. They are: vertical, horizontal, left-hand circular, and right-hand circular. Horizontal will be taken to mean that linear polarization which is parallel to the plane of the turnstile. The polarization of the turnstile is

$$P_R = \frac{1 - \dfrac{\cos[(\Pi/2)\sin\theta]}{\cos\theta}}{1 + \dfrac{\cos[(\Pi/2)\sin\theta]}{\cos\theta}}.$$

The incoming wave will have one of the four following values:

Polarization	P_w	D
Horizontal	1.0	0°
Vertical	1.0	θ
Left Circular	0	$\theta - \Pi/2$
Right Circular	∞	$\theta - \Pi/2$.

The total effective power of the turnstile antenna may be described as

Effective Relative Power = $P(\phi, \theta) * \Gamma(\theta)$.

Calculated and Measured Patterns

The formula for effective relative power was programmed into a digital computer to calculate values over the sphere for different polarizations. The output was arranged in a format similar to that of automatic pattern-recording equipment that would allow the comparison of calculated and measured patterns.

The pattern recording equipment output is called a radiation distribution plot (RDP) which has the form of typed numbers representing power expressed in decibels. The maximum is usually set at 2 with lower levels expressed as higher numbers. Only the even numbers are printed. The rows are in the ϕ direction (in the plane of the turnstile) and the columns are in the θ direction (about the plane of the turnstile). Normally, the power is sampled every 2° in the ϕ direction and every 5° in the θ direction.

Figures 1 through 4 are the computer-calculated patterns for the turnstile antenna using the effective relative power formula expressed in decibels, where dB = 10 log (Eff. Rel. Power). The computer output prints every decibel value. It is to be noted that the variation of the horizontal polarization pattern (in the plane of the turnstile), Fig. 1, is only 1 dB, although the highest level is 3 dB below the maximum power. This is because the polarization is circular when the angle is normal to the turnstile plane and hence 3 dB down, and only half the total power is available in the plane of the turnstile. Figure 2 shows the computer-calculated vertical polarization with its null in the plane of the turnstile. Figures 3 and 4 are the circular polarization patterns with the maximum signal on one pole and the null at the other pole. Figures 3 and 4 are mirror images of each other. The relative power is shown in Fig. 5. This is the pattern to be expected if the polarization is matched at every point that a sample is taken. Figure 6 is another form of Fig. 1 (horizontal polarization) showing the pattern in three-dimensional (3-D) format. This figure was drawn automatically by a CalComp plotter.

A simple turnstile antenna was constructed and tested in NRL's anechoic chamber to check the theory and to check on the suitability of the chamber for this type of measurement. Figures 7 through 10 show the RDP's obtained in the tapered-pyramid anechoic chamber. Figures 7 and 8 are the linear polarizations corresponding to Figs. 1 and 2, and Figs. 9 and 10 are the circular polarizations corresponding to Figs. 3 and 4. The antenna used consisted of four quarter-wave stubs mounted on a small sphere and fed in phase quadrature. Figures 7 through 10 are normalized and their maximum levels do not compare directly with Figs. 1 through 4. For Figs. 7 and 8, subtract 1 dB, and for Figs. 9 and 10 add 2 dB for direct comparison. These patterns show general agreement with the theory but they also point out some problems in the tapered-pyramid anechoic chamber. Tables 1 through 3 show comparisons between the computer printouts and the RDP's. For the circular polarizations and vertical polarization, the θ angles at several decibel levels are compared, whereas for the horizontal polarization the size of the 1-dB null area is compared. It is to be noted that the RDP output is subject to an error of ±1 dB as it is a digital device and that the angle increment is 5° in the θ direction and 2° in the ϕ direction. The horizontal polarization showed the best overall comparison (Fig. 11). In general, the levels were either the same or 5° off, which is the basic increment of the RDP. The circular polarization patterns point out one of the major deficiencies of the tapered pyramid anechoic chamber—its inability to propagate a good circularly polarized signal. As the signal level decreased the comparison difference grew larger and larger. When the turnstile antenna is rotated 180° it goes from one circular polarization sense to the other, and if the incoming wave is not circular a poor null will result.

The horizontal polarization patterns point out another problem in the anechoic chamber, the distorting influence of the antenna mount. In the ϕ direction the average error is only 3°, whereas in the θ angle, the upper boundary closest to the axis is in good agreement, while the lower boundary closest to the equator is off by an average of 17°. This is most probably due to the fiber-glass pole and metal head on which the antenna is mounted.

This page intentionally blank.

SEE ORIGINAL

COPY FOR

FIGURES

This page intentionally blank.

SEE ORIGINAL

COPY FOR

FIGURES

This page intentionally blank.

Page 10 blank

SEE ORIGINAL

COPY FOR

FIGURES

This page intentionally blank.

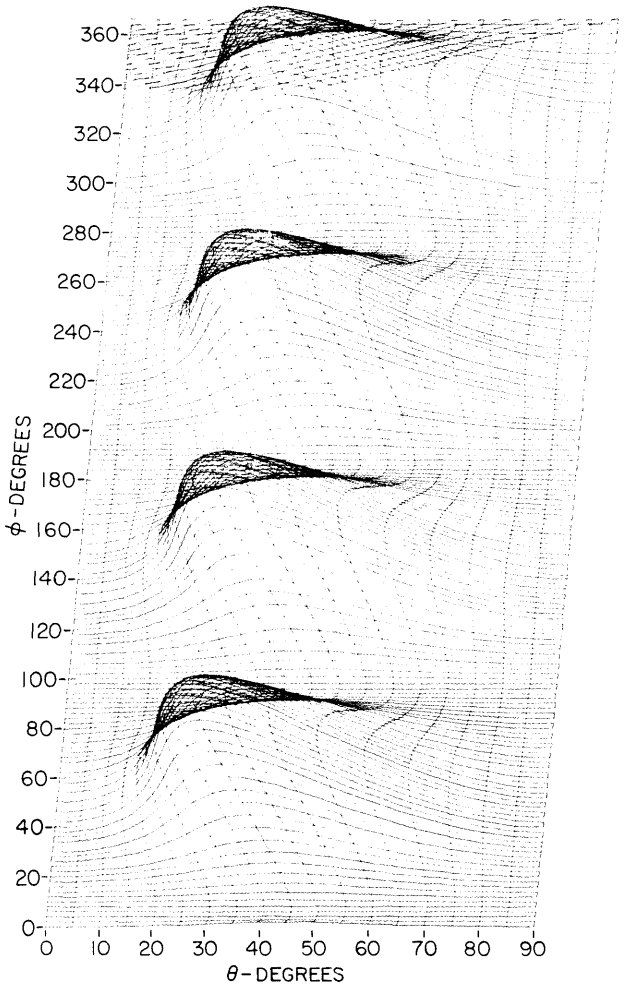

Fig. 6 - Computer 3-D plot, horizontal polarization

APPLICATION OF THE THEORY

Most satellites that use turnstile antennas have quarter-wave whip antennas placed symmetrically around the satellite. However, as the satellite becomes larger, the horizontal null deepens so that when a satellite is 3/8 of a wavelength in diameter the null is approximately 6 dB. Two satellite turnstile designs will be discussed; in the first, the traditional antenna is used in an unusual form, and in the second, the turnstile antenna is removed from the satellite, thus allowing a dramatic improvement over the conventional design.

Solar Explorer C

Solar Explorer C is a small 12-sided cylindrical satellite launched on July 8 1971. It is to be spin-stabilized with the spin axis pointing toward the sun. The top of the satellite is covered with solar experiments and there are four large panels covered with solar cells. This satellite will be launched in a 500-naut-mi orbit and will require an omnidirectional

This page intentionally blank.

SEE ORIGINAL

COPY FOR

FIGURES

This page intentionally blank.

SEE ORIGINAL

COPY FOR

FIGURES

This page intentionally blank.

Table 1
Pattern Comparison, Circular Polarization
(θ Direction)

Signal Level (dB)	Right Circular Fig. 10		Left Circular Fig. 9	Fig. 3 Computer (deg)	Average Error (deg)
	θ (deg)	180°- θ (deg)	θ (deg)		
0	180	0	0	0	0
-2	135	45	45	40	5
-4	105	75	65	60	10
-6	75	105	85	80	15
-8	50	130	100	95	20
-10	30	150	115	110	22
-12	10	170	125	125	22

Table 2
Pattern Comparison, Vertical Polarization
(θ Direction)

Signal Level (dB)	Fig. 8 Turnstile (deg)	Fig. 2 Computer (deg)	Error (deg)
0	0	0	0
-2	25	35	10
-4	40	45	5
-6	50	55	5
-8	60	65	5
-12	70	70	0
null	90	90	0
-12	105	105	0
-8	115	115	0
-6	125	125	0
-4	135	135	0
-2	140	145	5

Table 3
Horizontal Polarization; Location of Null Area

Figure Number	θ Angle (deg)	ϕ Angle (deg)	Degrees Subtracted from ϕ Angles
1 (Computer)	50-130	24-66	0
7 (RDP)*	50-160	20-70	0
7 (RDP)*	40-180	20-70	90
7 (RDP)*	60-150	24-66	180
7 (RDP)*	50-180	20-70	270
RDP Average	50-167	21-69	—
Error	0° 37°	1° 3°	—

*Each of the four null areas referenced to the first null area.

antenna. However, the presence of the solar cell panels would cause a serious distortion of the pattern of a set of antennas on the satellite. The solution to the problem was to make the solar cell panels do double duty as antennas. The panels were designed to be a quarter wavelength at the operating frequency and were electrically isolated from the rest of the satellite. Figure 12 shows a Solar Explorer mockup in the anechoic chamber.

Anechoic chamber tests show the two important changes in the antenna pattern of a satellite antenna as compared to a good turnstile antenna to be a deepening of the null in the horizontal polarization pattern and a shift in the phase quadrature caused by currents flowing on the skin of the satellite. Previous tests on spherical models show that the best null possible would be 4.2 dB below the maximum signal of the vertical polarization. It was necessary to mount the antennas 1-1/2 in. off center for structural purposes, and therefore a test was run to determine what effect this would have. Figure 13 shows an RDP for an on-center mounting with 5-dB nulls which shows little degradation due to a cylindrical rather than a spherical shape. The RDP's run on the Solar Explorer C mockup are shown in Figs. 14 through 17. Figure 14 shows the pattern with off-center mounting, which shows a slight directivity and 3-dB-deeper nulls caused by the off-center mounting. Figures 15, 16, and 17 show the other polarizations of the same model used for Fig. 14. Comparing these with Figs. 8, 9, and 10, respectively, it is noticed that the constant-level contours vary in θ as the rotation is in the ϕ direction. This is due to the deeper nulls on the equator ($\theta = 90°$) in the Solar Explorer C patterns.

Each solar cell panel has 7 dc wires connected to it, three for the power lines—plus, minus, and neutral—and four for two thermistors mounted at various points to monitor the temperature of the panel. Initial tests were run without the dc wiring on the panels. Tests run with the wiring and simulated solar cells showed that when the wires were not filtered, the patterns were quite distorted and unbalanced. To correct this problem, 1-μH chokes and feedthrough pi-type filters were mounted in the skin of the satellite, quite close to the solar cells, the chokes for high-input impedance, the filters for isolation. All three leads were kept short and symmetrical with respect to the other solar cells, and at least 3/8" from the skin before going through the filters. For the thermistor leads it was necessary to place a 100-μH choke in series with the leads in addition to the feedthrough filters, as the thermistor leads appeared to have a much tighter coupling to the panel then the solar cell wires. With all of these modifications the solar cell panels with wires produced antenna patterns identical to the plain panels (Fig. 18).

SEE ORIGINAL

COPY FOR

FIGURES

This page intentionally blank.

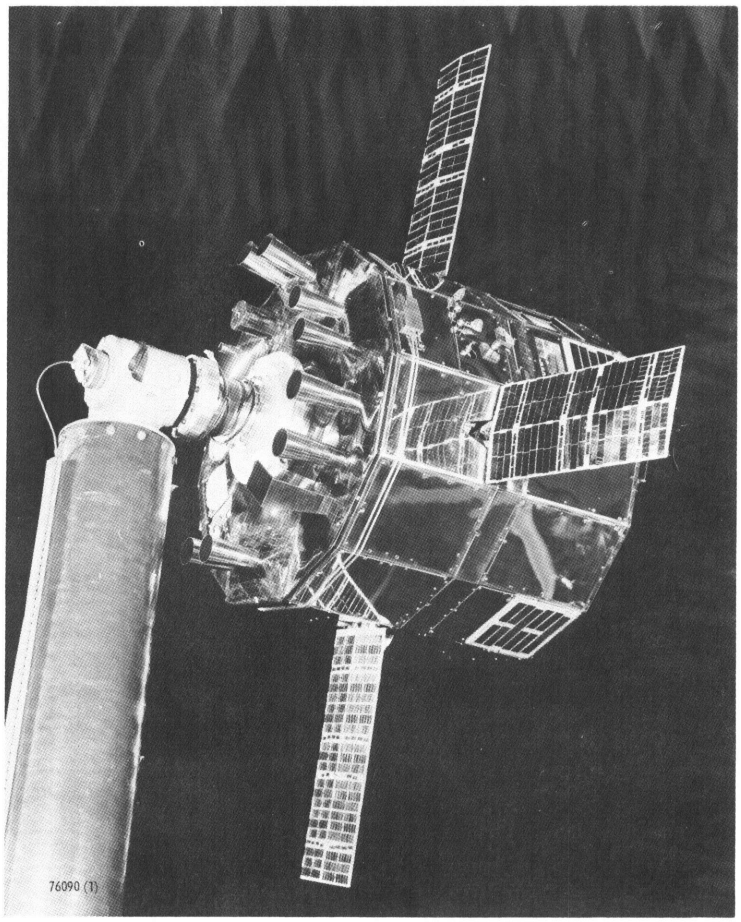

Fig. 12 - Solar Explorer C mockup

The antenna feed is very important to the success of this design. Since the panel is a quarter-wave long, the resistive component is close to 50 ohms but there is a large capacitive component due to the hinge design of the panel. This reactive component can be tuned out with a shunt capacitance to bring the VSWR to below 1.5 to 1 as the antenna has to be operated over only a 10% bandwidth.

The details of the solar cell hinge design, including the placement of the rf and dc wires, and the installation and testing of the solar cell antenna on the flight model satellite were performed by other investigators and will be reported later.

Turnstile on a Boom

An NRL satellite launched in October 1969 required a new approach to improve the rf performance. This satellite is gravity-gradient stabilized in a 500-naut-mi orbit with the south pole always pointing toward the earth. The satellite is multifaceted and egg-shaped, about 27 in. in diameter and 33 in. high. It has 60 major facets, most of which are covered with solar cells. The telemetry operates in the 136- to 138-MHz band. Figure 19 is an artistic sketch of the multifaceted satellite showing the antennas and the magnetometer boom (which is mostly nonconductive).

This page intentionally blank.

SEE ORIGINAL

COPY FOR

FIGURES

This page intentionally blank.

SEE ORIGINAL

COPY FOR

FIGURES

This page intentionally blank.

SEE ORIGINAL

COPY FOR

FIGURES

This page intentionally blank.

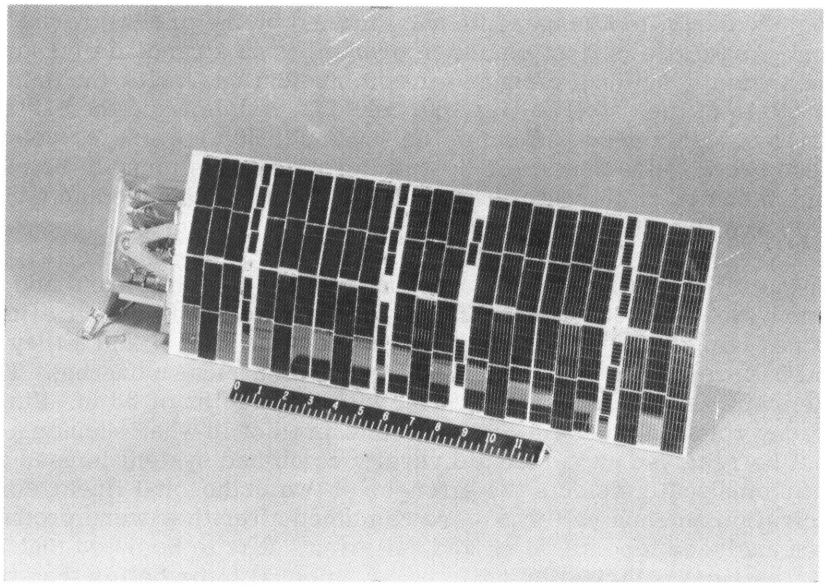

Fig. 18 - Modified solar cell panels

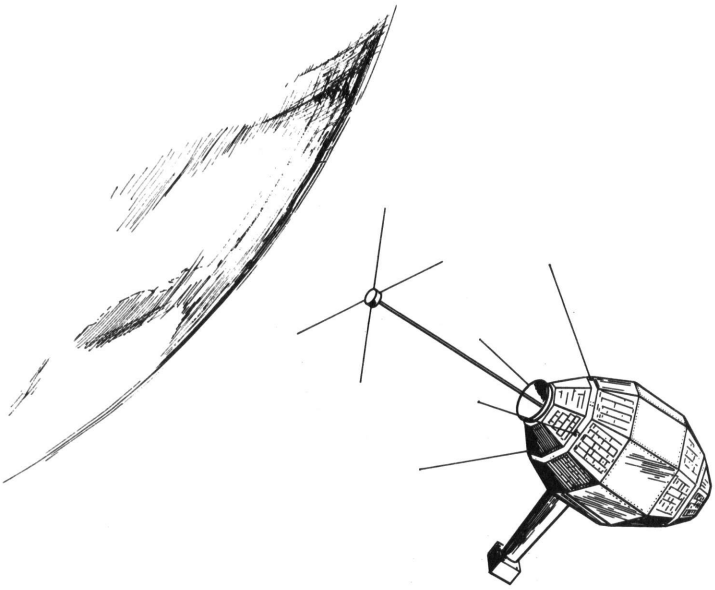

Fig. 19 - Multifaceted satellite with boom antenna

The antenna requirements for the satellite are dictated by the orbital dynamics of stabilization. When the satellite is first placed in orbit, it is in a random orientation and therefore requires an omnidirectional antenna for communication. After the satellite is stabilized only the bottom of the satellite ($\Theta = 180° \pm 60°$) is visible from the earth, which would require an antenna with a good pattern in the $\Theta = 180° \pm 60°$ region, for communication. To satisfy these two requirements, the best arrangement was found to be two turnstile antenna systems, one mounted on the satellite itself and the other mounted on a boom projecting downward from the satellite.

The antenna on the satellite was mounted midway between the belly band and the top, and at a 45-deg angle with respect to the horizontal plane. The linear polarization antenna patterns are shown in Figs. 20 and 21 and when compared with Figs. 7 and 8 they show large null shifts and pattern distortions caused by the asymmetrical mounting. The null depths are about the same as for a spherical model with a diameter of 33 in. Since the phenomenon of Faraday rotation makes it impossible to predict in what manner a linear polarization can best be received and since a diversity combined system is used at the ground station that automatically selects the stronger of two orthogonal linear components, the two linear polarization antenna patterns were combined after they were produced and the combined pattern analyzed for null depth and null area. It is to be noted that in a good turnstile antenna the vertical polarization will always be equal to or better than the horizontal polarization. For this antenna the combined null depth was 10 dB over the whole sphere, with approximately 1.5% of the pattern area below 7 dB. The 10-dB nulls occurred around the south pole so that when the satellite is stabilized, the worst part of the pattern is in view.

To increase the effective radiated power of the satellite it was decided to try a turnstile antenna on a boom projecting down from the satellite. A set of reflectors was also tried on the boom antenna. Tests were run on a sheet-metal model to determine the optimum length. Factors to consider included isolation between the two turnstile antennas and the effect of reflections on the satellite itself. Boom lengths of 3 to 5 ft in 6-in. increments were tried with the results shown in Fig. 22. The combined null depth was at a minimum at 4 ft (Fig. 22A); the null percentage was also at a minimum at 4 ft (Fig. 22B), climbing steeply at 5 ft where the satellite acted like a reflector and made the pattern directional. When the satellite was stabilized the minimum null depth was 3 dB at 3-1/2 ft and 5 dB at 4 ft (Fig. 22C). The isolation between the two antennas increased smoothly as the separation increased (Fig. 22D). As a compromise of all of these factors, a flight boom length of 4 ft was chosen.

The idea of deliberately giving the boom antenna some directivity was studied. It would have the advantages of a higher effective radiated power, less influence of the satellite on the antenna pattern, and a higher isolation from one antenna to the other. The directivity was obtained by putting a crossed reflector behind the turnstile on a 4-3/4 ft-long boom. The reflector was 14% longer than the boom antenna and mounted 1/8 of a wavelength behind the turnstile. This antenna had a pattern as shown in Fig. 23 (which is a decibel plot) with a 3-dB gain over the turnstile antenna, a 6-dB beamwidth of 120 deg, and a front-to-back ratio of 8 dB. Thus at the extreme angles of a stabilized satellite, the signal would be -3 dB with respect to a standard turnstile as compared with the -5 dB of the turnstile on a boom. However, if stabilization is lost, a directional boom antenna will be less effective and therefore this design was not used.

Antenna patterns (RDP's) were run on the boom antenna and are shown in Figs. 24, 25, and 26. Figure 24, when compared with Fig. 7, shows null shifts and pattern distortion caused by the influence of the satellite. Figure 25 compares very well with Fig. 8, although the cross-polarization null at the equator ($\theta = 90°$) is not quite as sharp as in Fig. 8. Figure 26 is the circular polarization of interest to a stabilized satellite. When compared to Fig. 9, it can be seen that as the signal level decreases (becomes cross polarized) the difference between the two widens. The comparisons between the patterns are tabulated in Tables 4 through 6.

SEE ORIGINAL

COPY FOR

FIGURES

This page intentionally blank.

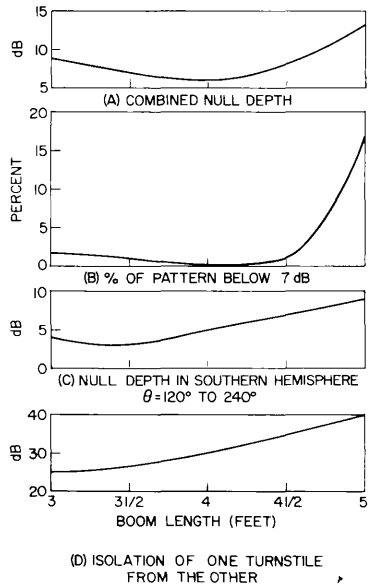

Fig. 22 - Antenna parameters vs. boom length

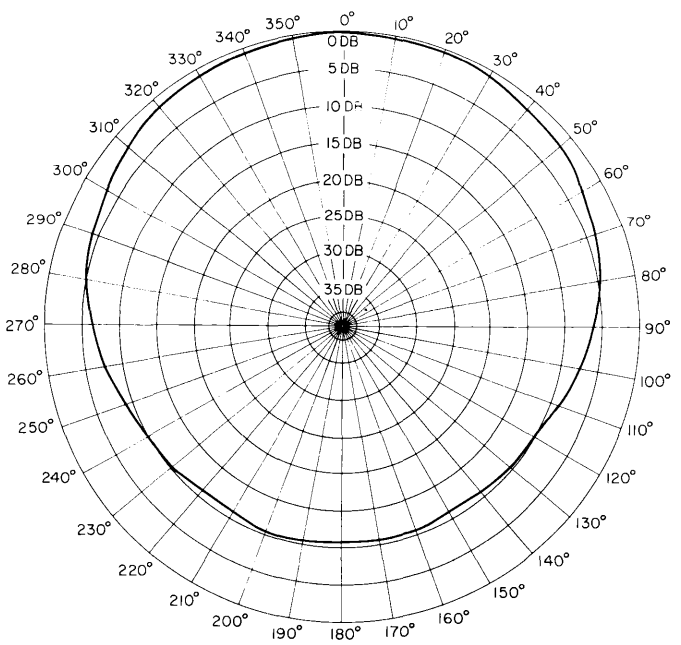

Fig. 23 - Polar pattern, turnstile with reflector

This page intentionally blank.

SEE ORIGINAL

COPY FOR

FIGURES

This page intentionally blank.

SEE ORIGINAL

COPY FOR

FIGURES

This page intentionally blank.

Table 4
Boom and Turnstile Antenna Comparison,
Vertical Polarization

Signal Level (dB)	Boom Antenna (Fig. 24) (deg)	Turnstile Antenna (Fig. 8) (deg)	Difference (deg)
0	0	0	0
-2	15	25	10
-4	30	40	10
-6	40	50	10
-8	60	60	0
null	90	90	0
-8	120	115	5
-6	130	125	5
-4	150	135	15

Table 5
Boom and Turnstile Antenna Comparison,
Left Circular Polarization

Signal Level (dB)	Boom Antenna (Fig. 25) (deg)	Turnstile Antenna (Fig. 9) (deg)	Difference (deg)
0	180	180	0
-2	155	135	20
-4	115	110	5
-6	80	75	15
-8	75	50	30
-10	70	30	40
-12	65	10	55

The boom turnstile antenna had a null depth of 7 dB over the whole sphere and of 4 dB in the area observed on a stabilized satellite. Thus by using a boom antenna the effective radiated power was increased and the null depth decreased.

After the multifaceted satellite was launched a unique opportunity was presented to measure the performance of the satellite boom antenna and compare that with its performance as measured in the anechoic chamber. The axial ratio was chosen as a parameter that could be accurately measured and compared. From the antenna patterns it was known that the polarization was linear near the equator and circular on the bottom. A 60-ft parabolic antenna was instrumented as shown in Fig. 27 to measure the polarization. Figure 28 shows three representative ellipses of the satellite as it moved from the horizon toward the overhead position. Also in Fig. 28 are the corresponding three ellipses of a model tested in the anechoic chamber. Figure 29 is a graph of the axial ratio of the photos, and shows very good agreement.

Table 6
Boom and Turnstile Antenna Comparison,
Horizontal Polarization—Location
of Null Area

Figure Number	θ Angle (deg)	ϕ Angle
7 (Average)	50-167	21-69
23	40-55	-10 to 20
23 (ϕ-90°)	40-60	20-60
23 (ϕ-180°)	30-50	10-40
23 (ϕ-270°)	50-70	30-60
Average Error	10-107	0-24

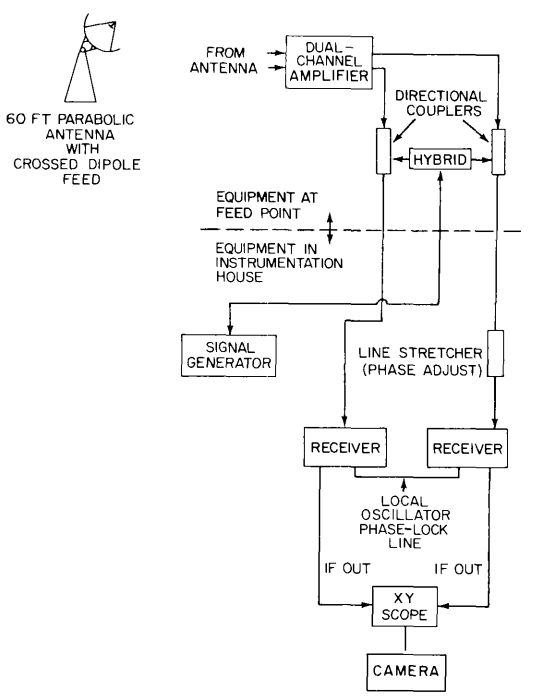

Fig. 27 - VHF instantaneous polarimeter

ANOTHER APPROACH

Up to this point vhf antennas that do not take into account the orbital dynamics of the satellite have been discussed. In this section, the results of a detailed study of the orbital parameters will be presented, along with a novel antenna to match the orbital parameters.

Orbital Analysis

There are three important areas to consider in the design of a low-altitude satellite antenna system designed to take advantage of the orbit. They are the change in path length

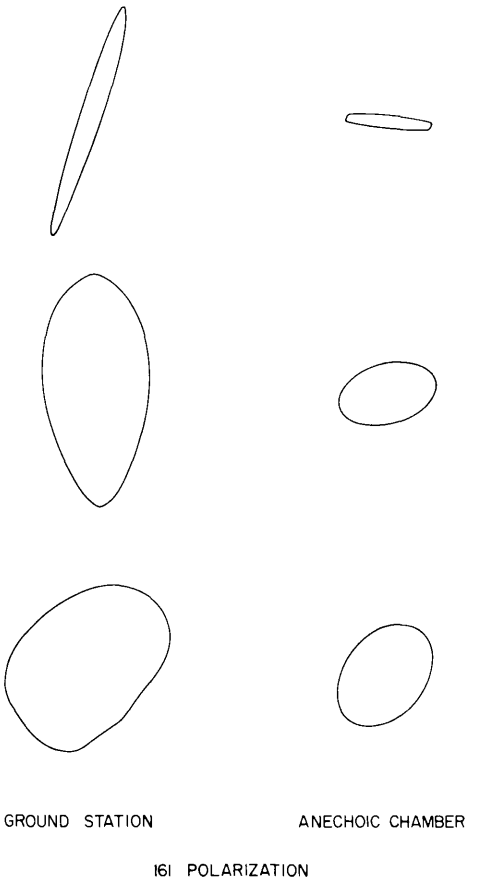

Fig. 28 - Axial ratios of Multifaceted satellite, measured in anechoic chamber and in flight

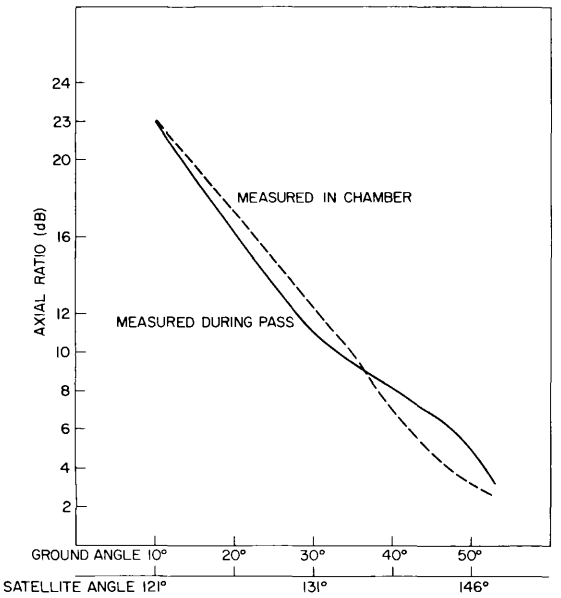

Fig. 29 - Axial ratios of boom antenna

as the satellite passes from the horizon to overhead, the time of transit at high angles, and the distribution of maximum elevation angles.

In a 500-naut-mi satellite, the path length at the horizon is 1930 mi, while overhead it is 500 mi. The ratio of signal received to signal transmitted is expressed in the Friis transmission formula as

$$\frac{P_R(\theta, \phi)}{P_A(\theta, \phi)} = \frac{\lambda^2}{(4\pi)^2} \frac{G_R G_T}{R^2},$$

where λ is the wavelength, G is the antenna gain, and R is the range. From this formula it can be seen that the difference in signal strength between the satellite on the horizon and the satellite overhead is 11.7 dB. Figure 30 is a plot of the increase in signal strength vs. elevation angle. This plot shows a 7-dB increase in signal when the ground elevation changes from 0° to 30° and a change of 10.5 dB from 0° to 60°, with only a 1-1/2 dB improvement from 60 to 90°.

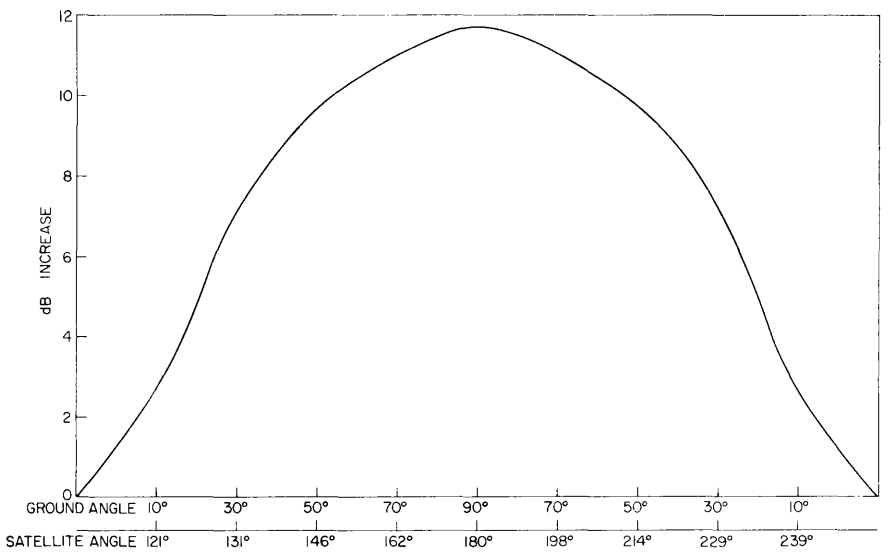

Fig. 30 - Change in signal strength due to range change

It is of interest to know the transit time at high angles. One pass studied had a maximum elevation angle of 87°. This pass took a total of 17 min to go from horizon to overhead to horizon; 68 sec of this time the elevation angle was over 70°, and for 45 sec the elevation angle was over 80°. Figure 31 is a plot of this pass.

An extensive analysis of orbital elevation angles was conducted with the aid of a digital computer. A satellite tracking program, using orbital elements of a recently launched multifaceted satellite with a boom antenna, was run to produce 560 passes over a period of 85 days. These passes were for a southern Maryland site with a latitude of 38.5°. Additional computer runs were made for latitudes from 0° to 90°. This satellite was launched in a 498-naut-mi circular orbit with an inclination of 70°. The results for a latitude of 38.5° are summarized in Table 7. It is assumed that any pass with a maximum elevation angle less than 5° would not be tracked. There are on the average 39.0

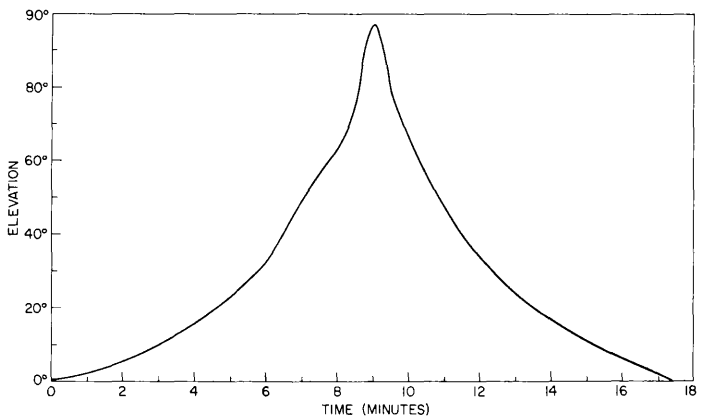

Fig. 31 - Elevation angle vs. time

Table 7
Statistical Study of Satellite Elevation Angles

Maximum Elevation Angle in Passes (deg)	Total Number of Passes	Passes per Week	Percent of Total	Percent of 5°-90°
0-4	85	7	15.0	—
5°-30	273	22.5	49.0	57.5
31-60	129	10.6	23.0	27.1
61-90	73	6.0	13.0	15.4
61-70	26	2.1	4.6	5.5
71-80	26	2.1	4.6	5.5
81-90	21	1.8	3.8	4.4
86-90	7	0.6	1.2	1.5
5-90	475	39	85	100
0-90	560	46	100	—
5-70	428	35.3	76.5	90
0-70	513	42.2	91.5	—

passes per week with a maximum elevation between 5° and 90° of which an average of 35.3 passes are between 5° and 70° with only 10% above 70° and only 1.5% above 85°. The three highest passes during the 85-day period studied were 88.9°, 87.8°, and 87.6°.

The results of the study of satellite passes vs. latitude are shown in Fig. 32. The solid line shows the variation of the percentage of passes with a maximum elevation below 30°, and the dashed line shows the total number of passes per day seen at a given latitude. Note that the percentage of 30° or lower elevation passes is relatively constant until a latitude of 50° is reached. The percentage of passes with maximum elevation over 60° is also relatively constant (between 13.1 and 15.2%) over this range. As the latitude corresponding to the inclination is reached, the number of high-angle passes increases dramatically and then drops off as higher latitudes are analyzed. The total number of passes increases from a minimum at the equator to a maximum (a pass every revolution) at the North Pole. This analysis shows that Table 7 will be accurate for ground stations in the United States with latitudes of 25 to 49° but would not be accurate for higher latitudes.

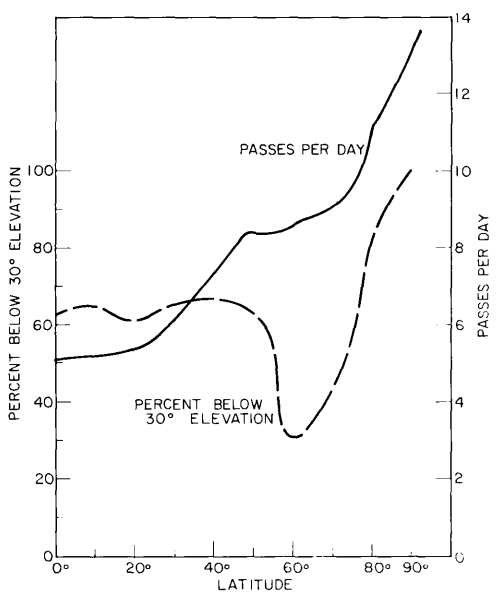

Fig. 32 - Satellite pass parameters vs. latitude

In summary, most of the passes are at low angles, with about one pass every two weeks with a maximum elevation above 85° and during this pass, the satellite will spend about 45 sec with an elevation angle greater than 80°.

The Array Antenna

A new dual-input directional antenna has been developed to take advantage of the orbital parameters and to optimize the signal coming from a gravity-gradient-stabilized satellite. This antenna has been designed and tested to meet space requirements and is believed to be far superior to any other technique. This antenna offers the advantages of dual input, gain, high front-to-back ratio, omnidirectivity in the azimuth plane, and compact storage during launch. Figure 33 is a photo of the prototype model. The array consists of four antennas arranged as a loop. Each antenna consists of a dipole with a reflector. The whole assembly is collapsible into a size not much larger than the turnstile

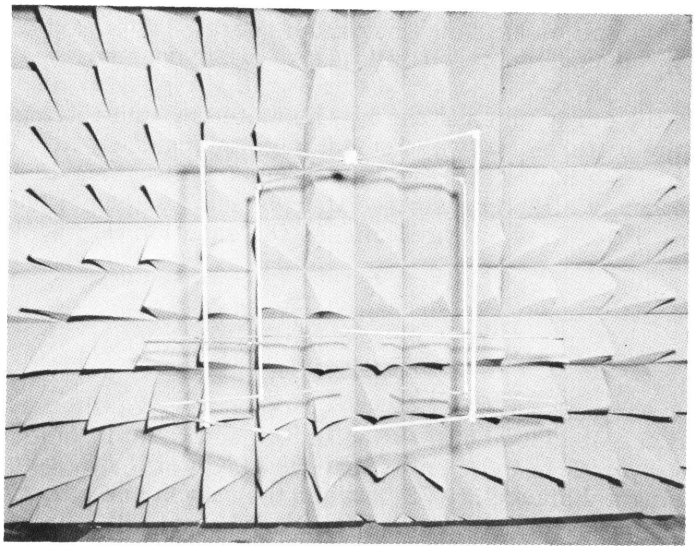

(a)

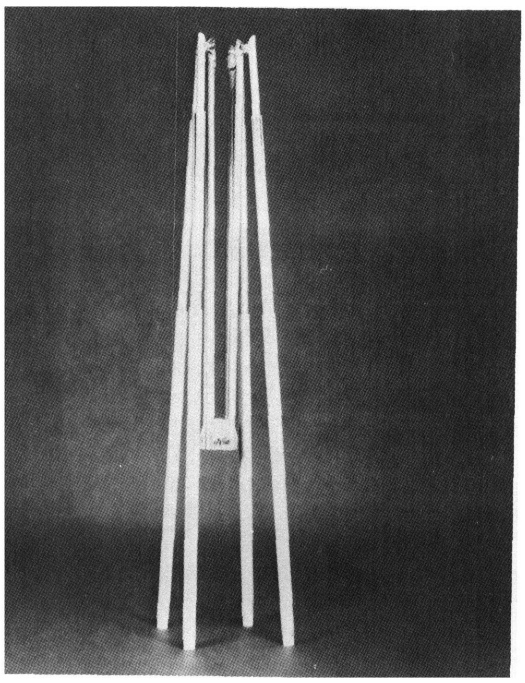

(b)

Fig. 33 - Array antenna

antenna on a boom. The four elements are driven with a six-port hybrid (two inputs, four outputs, each output 90° out of phase with respect to each other). Opposing antennas are oriented to have the same sense, but are fed 180° out of phase. The net result is a difference pattern, with a null on axis and maximum energy 45° off axis. The energy to the rear is drastically reduced compared with that of other designs.

The directivity of the array antenna can be calculated by multiplying the pattern of two point sources by the pattern of a two-element yagi antenna. By spacing two point sources slightly more than a half-wavelength apart and feeding them 180° out of phase with respect to each other, a slightly distorted figure-eight pattern is obtained with peaks 45° from the null. For a two-element yagi antenna the equation is given as

$$E(\theta) = 1 + \frac{Z_{12}}{Z_{22}} \angle \xi + d_u \cos \theta,$$

where Z_{12} is the mutual impedance, Z_{22} is the self-impedance of the parasitic element, $d_u = 2\pi d/\lambda$, where d is the distance between the driven and parasitic elements, $\xi = \Pi\tau_m$ where $\tau_m = \arctan X_{12}/R_{12}$. It is to be noted that the length of the driven element does not affect the pattern. Using a distance of $\lambda/8$ between the driven and parasitic elements, S. Uda gives a value of approximately 5 ohms (real). The parasitic element was chosen to be approximately 195° long, giving Z_{12} a large reactive component. This gives a yagi design with a front-to-back ratio of 12 dB. The complete formula for the array antenna is

$$E(\theta) = \cos\left(\frac{s}{2}\sin\theta + \frac{\tau}{2}\right)\left[\left(1 + \left|\frac{Z_{12}}{Z_{22}}\right|\sin\Psi\right)^2 + \left(\left|\frac{Z_{12}}{Z_{22}}\right|\cos\Psi\right)^2\right]^{1/2},$$

where

$$\Psi = \Pi + \arctan\left|\frac{X_{12}}{R_{12}}\right| + \frac{2\Pi d}{\lambda}\cos\theta,$$

τ = phase difference at feed point.

In the azimuthal rotation (about the equator of the satellite) the array is approximately omnidirectional with a variable polarization. These parameters can be calculated using the array formula, the dipole formula, and the polarization formula, all previously discussed in this report. Consider each parallel set of antennas as an element and the voltage pattern of each pair can be labeled as E_1 and E_2, respectively. The azimuthal pattern will be calculated at an angle of 40° off the polar axis in the main beam of the array pattern. The 0° angle will be taken as a point which is parallel to one set of antennas and perpendicular to the other set.

The polarization factor P can be expressed as

$$P = \frac{E_1 - E_2}{E_1 + E_2},$$

and P varies from 1.0 (linear) at an angle of 0° to 0.28 (elliptical) at an angle of 45°. This is because, at an angle of 0°, the parallel antennas are in the null position with a resultant linear polarization, while at the corners of the array, all four antennas contribute to the signal level and the signal is almost circular in polarization.

The formulas for incoming waves are

$P = E_1^2$ for an incoming linear wave,

$P = 1/2\ (E_1 + E_2)^2$ for an incoming linear wave,

where

$$E_1 = E\ (\theta - 90°)$$

$$E_2 = E(\theta)\ \frac{\cos\ [(\Pi/2)\cos\theta]}{\sin\theta},$$

where $E(\theta)$ is the array formula. These two formulas are plotted in Fig. 34 which shows a variation of 1.8 dB for the linear case, while the circular polarization is 0.85 to 8.3 dB worse than the linear polarization. Linear polarization would be the most desirable polarization for the ground station link to the array antenna. As was previously mentioned, a diversity combined system would eliminate the problem of the Faraday rotation.

The array antenna was tested extensively in the anechoic chamber. It was found to have a gain of 2 dB at a point 45° off axis and a 3-dB beamwidth of 50° on each side of the polar axis for a total of 100-deg beamwidth. This leaves a small cone on axis where the signal level will be low, but as was previously mentioned, the satellite is seldom seen in this area. The average backlobe level is -21 dB with a 40-dB null on axis. Figure 35 is the measured antenna pattern and the theoretically calculated pattern of the array. The direction to the ground station is toward the bottom of the page. The measured pattern of Fig. 35 was taken at an azimuth angle of 0°. At this angle, a direct comparison between a standard gain dipole and the array indicated a gain of 2 dB over isotropic at this angle. Since this is the lowest signal level in the azimuthal plane, it is the lowest gain of the angles of interest in the array antenna.

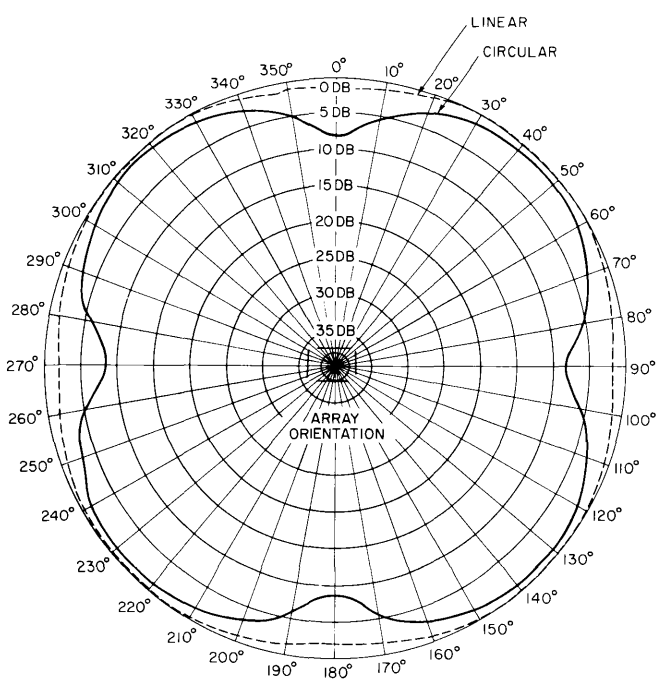

Fig. 34 - Azimuth antenna pattern, array antenna

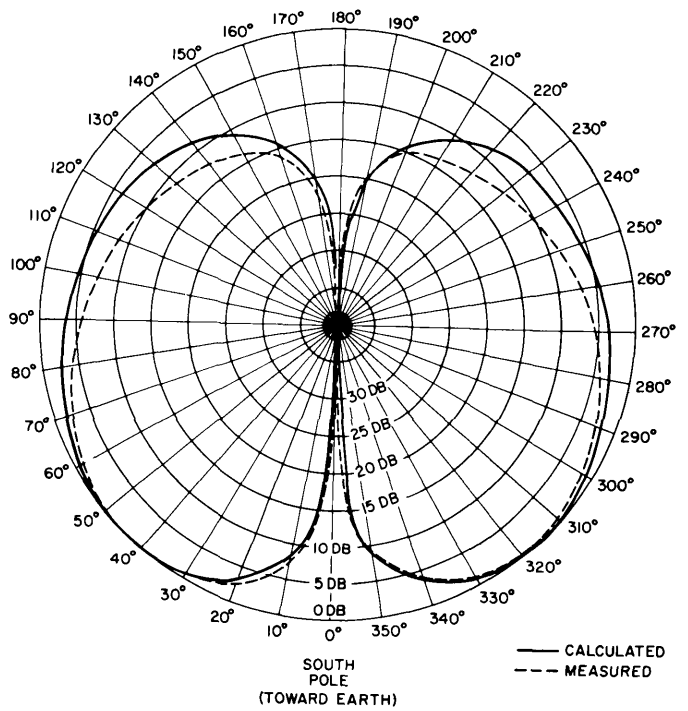

Fig. 35 - Polar antenna pattern, array antenna

Array Summary

Three of the antennas discussed in this report will be compared and the results summarized. These antennas are the ones that are on a boom extending away from the satellite. They are the turnstile, the turnstile with reflectors, and the array antennas. The antenna patterns of these three antennas (Figs. 24, 23, and 35) were converted from satellite coordinates to ground station coordinates and combined with the range change graph (Fig. 30), and then plotted in Fig. 36 to give the relative signal strength vs. elevation angle. This plot shows the superiority of the array antenna.

In the 0° to 30° elevation range where 64% of the passes occur, the turnstile with reflectors is an average of 2.0 dB better than the turnstile and the array is 2.6 dB better than the turnstile. In the 5° to 60° elevation range where 71% of the passes occur, the turnstile with reflectors is an average of 2.9 dB better than the turnstile, and the array is 3.2 dB better. At an angle of 85° the signal strength from the array will be equal to that at the horizon; passes above this angle will be poor; however, the period of the poor signal will be poor (less than a minute out of a 17-min pass).

In the 0° to 70° elevation range which will cover 91% of all passes, the array will be superior to the turnstile by 0 to 5 dB with an average improvement of 3.2 dB. From 0° to 50° the array is superior to the turnstile with reflector and the front-to-back ratio of the array is clearly superior to all other antenna types which will minimize rfi problems in the satellite.

CONCLUSION

This report has shown that a good mathematical model of the turnstile antenna can be developed and that there is good correlation between this model and tests run in the

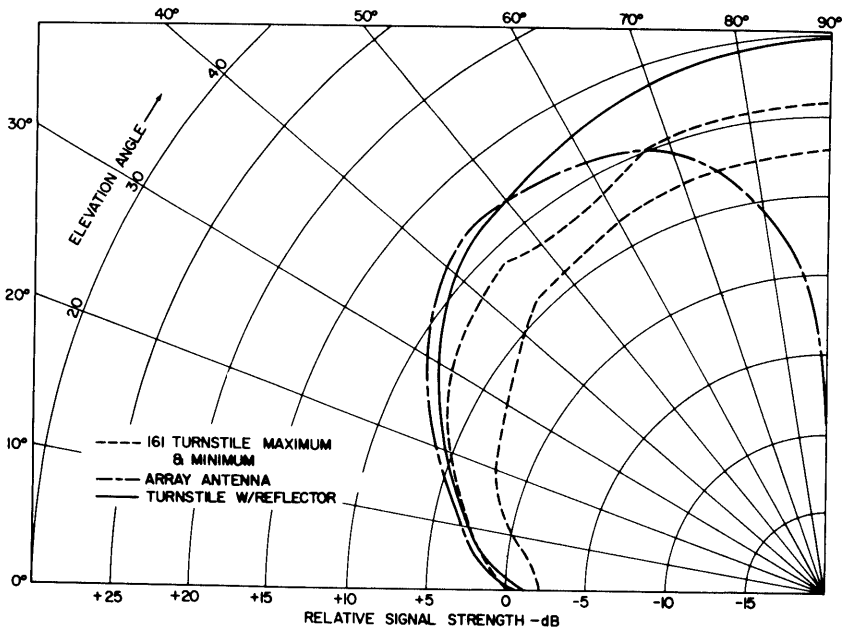

Fig. 36 - Signal strength patterns for three antennas

anechoic chamber. With more study and analysis this theory could probably be extended to predict patterns for actual satellites, thus allowing optimization of the satellite before testing begins. The mathematical model shows that there are limits to the accuracy of the anechoic chamber and that some measurements must be taken with great care to avoid misleading results.

The two satellites discussed showed that novel applications can extend the usefulness of the turnstile antenna to satellites where the traditional turnstile simply did not work. The Solar Explorer C in particular presented an extremely difficult problem which was solved by making the solar cell panels and the antennas one and the same. The turnstile on a boom allowed transmitter and receiver problems to be separated with improved patterns and simplification of internal rf cable and filter harnesses.

And finally, a study of the orbits of the satellites produced an optimized antenna design that offers an average improvement of 3.2 dB over the best existing designs. This design allows the simultaneous connection of a transmitter and receiver and doubles the effective radiated power of the satellite. It offers the best fit to the requirements for a vhf antenna for a low-altitude satellite which includes a pattern taper to match the change in signal strength during a pass, has a good front-to-back ratio, is erectable in space, and has omnidirectivity in the azimuthal plane.

ACKNOWLEDGMENTS

The author gratefully acknowledges the guidance of Lenard Hearton for his support of engineering principles; Porter Lyon for many helpful suggestions; Philip McCray and Henry Rogers, who assisted in running the tests on which this report is based; and James Trexler for his encouragement to write this report.

BIBLIOGRAPHY

Blake, L.V., "Antennas," New York:Wiley, 1966, p. 327, 331

Brown, G.H., "The 'Turnstile' Antenna," Electron. 9 (No. 4):14-17, 48

Eisele, J.A., "Astrodynamics, Rockets, Satellites and Space Travel," Washington:National Book Company, 1967, p. 270

Gruenberg, E.L. (ed.), "Handbook of Telemetry and Remote Control," New York:McGraw-Hill, 1967, Ch. 16

Hollis, J.S., Lyon, T.J., and Clayton, L., Jr., "Microwave Antenna Measurements," Sci. Atlanta 1969, Ch. 3

Jasik, H. (ed.), "Antenna Engineering Handbook," New York:McGraw-Hill, 1961, p. 3-4

Korvin, W., and Jackson, R.B., "Antennas for Space Vehicles," Space/Aeronaut. 42 (No. 6): 60-67 (Nov. 1964)

Kraus, J.D., "Antennas," New York:McGraw-Hill, 1950, pp. 54, 318, 424

Kraus, J.D., "Radio Astronomy," New York:McGraw-Hill, 1966, p. 143

Marsten, R.B. (ed.), "Communication Satellite Systems Technology," New York:Academic Press, 1966, p. 347

Nichols, S., "Satellite Turnstile Antennas," NRL Report 6907, Aug. 6, 1969

"Reference Data for Radio Engineers," 5th edit., Indianapolis:Howard W. Sams, 1968, pp. 25-36

Uda, S., and Mushiake, Y., "Yagi-Uda Antenna," Sendai, Japan:Research Institute of Electrical Communication of the Tohoku University, 1954, p. 70

Welch, G.V., "Wave Propagation and Antennas," Princeton, N.J.:Van Nostrand, 1958, p. 177

Appendix

GLOSSARY OF SYMBOLS AND TERMS

Anechoic chamber	Room in which outer space is simulated for an rf environment
Axial ratio	Measure of polarization circularity
dB	Decibels (relative, unless noted)
D	Polar angle of separation
$E, E(\phi), E(\theta)$	Electric field
G	Antenna gain
Horizontal polarization	In plane of turnstile or satellite equator, ϕ direction
Left circular polarization	Polarization of turnstile looking from above ($\theta = 0°$)
MHz	Megahertz
Orbital elements	Key parameters that describe a satellite orbit supplied by the Naval Space Surveillance System
P	Polarization factor
$P(\phi,\theta)$	Power received
r	Distance
R_{xx}	Resistance
RDP	Radiation Distribution Plot (3-D antenna pattern)
Right circular polarization	Polarization of turnstile looking from below ($\theta = 180°$)
X_{xx}	Reactance
Z_{xx}	Impedance
Null %	Percentage of RDP area below 7 dB
Vertical polarization	About the axis of the turnstile, θ direction
Γ	Polarization efficiency
ξ	Impedance phase angle
θ	Angle about the axis of turnstile on satellite equator
λ	Wavelength
τ	Phase difference
ϕ	Angle in plane of turnstile
ψ	Yagi phase angle

Security Classification

DOCUMENT CONTROL DATA - R & D

(Security classification of title, body of abstract and indexing annotation must be entered when the overall report is classified)

1. ORIGINATING ACTIVITY *(Corporate author)* Naval Research Laboratory Washington, D.C. 20390	2a. REPORT SECURITY CLASSIFICATION Unclassified 2b. GROUP

3. REPORT TITLE

VHF ANTENNAS FOR LOW-ALTITUDE SATELLITES

4. DESCRIPTIVE NOTES *(Type of report and inclusive dates)*
An interim report on one phase of the problem.

5. AUTHOR(S) *(First name, middle initial, last name)*

Stephen Nichols

6. REPORT DATE July 12, 1971	7a. TOTAL NO. OF PAGES 56	7b. NO. OF REFS 14

8a. CONTRACT OR GRANT NO. NRL Problems A01-17 and A01-20 b. PROJECT NO. Project A37-538-002/652-1/F019-01-01 c. d.	9a. ORIGINATOR'S REPORT NUMBER(S) NRL Report 7292 9b. OTHER REPORT NO(S) *(Any other numbers that may be assigned this report)*

10. DISTRIBUTION STATEMENT

Approved for public release; distribution unlimited.

11. SUPPLEMENTARY NOTES	12. SPONSORING MILITARY ACTIVITY Department of the Navy (Naval Air Systems Command), Washington, D.C. 20360 Department of the Air Force

13. ABSTRACT

Two vhf satellite antennas are discussed in depth. The first is a turnstile antenna, which is presented with theory, computer calculations, experimental results, and two novel applications. The first application solves the problem of interfering solar cell panels by combining them with the antenna. The second application puts the turnstile antenna on a boom away from the satellite to minimize interference.

The second vhf satellite antenna presented has multiple elements and is designed to optimize the pattern with respect to the distance and angle from a stabilized satellite to a ground station as it passes overhead. This antenna was found to have a 3-dB improvement over the best turnstile designs.

DD FORM 1 NOV 65 1473 (PAGE 1)

S/N 0101-807-6801

Security Classification

Security Classification

14. KEY WORDS	LINK A ROLE	LINK A WT	LINK B ROLE	LINK B WT	LINK C ROLE	LINK C WT
Circular polarization						
Computer antenna patterns						
Communications satellite, multifaceted						
Horizontal polarization						
Solar Explorer C						
Spacecraft antennas						
Vertical polarization						
Vhf antennas						
Turnstile antenna						
Yagi antenna						

DD FORM 1 NOV 65 1473 (BACK)
(PAGE 2)

Security Classification